

## Article

# Haploinsufficiency of the TDP43 ubiquitin E3 ligase RNF220 leads to ALS-like motor neuron defects in the mouse

Pengcheng Ma<sup>1,†</sup>, Yuwei Li<sup>1,2,†</sup>, Huishan Wang<sup>1,2</sup>, and Bingyu Mao<sup>1,3,\*</sup>

<sup>1</sup> State Key Laboratory of Genetic Resources and Evolution, Kunming Institute of Zoology, Chinese Academy of Sciences, Kunming 650223, China

<sup>2</sup> Kunming College of Life Science, University of Chinese Academy of Sciences, Kunming 650203, China

<sup>3</sup> Center for Excellence in Animal Evolution and Genetics, Chinese Academy of Sciences, Kunming 650223, China

<sup>†</sup> These authors contributed equally to this work.

\* Correspondence to: Bingyu Mao, E-mail: mao@mail.kiz.ac.cn

Edited by Zhen-Ge Luo

**TDP43 pathology is seen in a large majority of amyotrophic lateral sclerosis (ALS) cases, suggesting a central pathogenic role of this regulatory protein. Clarifying the molecular mechanism controlling TDP43 stability and subcellular location might provide important insights into ALS therapy. The ubiquitin E3 ligase RNF220 is involved in different neural developmental processes through various molecular targets in the mouse. Here, we report that the RNF220<sup>+/-</sup> mice showed progressively decreasing mobility to different extents, some of which developed typical ALS pathological characteristics in spinal motor neurons, including TDP43 cytoplasmic accumulation, atrophy, muscle denervation, and atrophy. Mechanistically, RNF220 interacts with TDP43 *in vitro* and *in vivo* and promotes its polyubiquitination and proteasomal degradation. In conclusion, we propose that RNF220 might be a modifier of TDP43 function *in vivo* and contribute to TDP43 pathology in neurodegenerative disease like ALS.**

**Keywords:** TDP43, RNF220, amyotrophic lateral sclerosis (ALS), polyubiquitination

### Introduction

Protein quality control mediated by the ubiquitin proteasome system (UPS) is vital for the regulation of cellular homeostasis (Swatek and Komander, 2016). Impairment of the UPS has been implicated in many neurodegenerative diseases, including amyotrophic lateral sclerosis (ALS), Parkinson's disease, Alzheimer's disease, and polyglutamine disease, due to accumulation of toxic proteins in neurons or glial cells (Tashiro et al., 2012; Galves et al., 2019). As the enzyme that confers specificity to the ubiquitination cascade, the importance of ubiquitin E3 ligases is increasingly recognized in neurodegeneration (Swatek and Komander, 2016; Galves et al., 2019). RNF220 was firstly identified as an ubiquitin E3 ligase for

Sin3B (Kong et al., 2010). Recently, we reported that RNF220 modulates Shh/Gli signaling through targeting Glis for K63-linked polyubiquitination and thus is involved in early neural patterning during vertebrate embryo development (Ma et al., 2019). It is also involved in the development of the cerebellum and the locus coeruleus through targeting EED and Phox2a/b, respectively (Ma et al., 2020a; Song et al., 2020). In neural stem cells, loss of RNF220 inhibits cell proliferation and promotes cell differentiation *in vitro* (Zhang et al., 2020). However, whether RNF220 plays a role in neurodegenerative disease progression is unknown.

ALS is a devastating neurodegenerative disease, characterized by degeneration of motor neurons, muscle weakness, and denervation, which has been causally associated with mutations in a large number of genes with distinct functions (Dion et al., 2009; Taylor et al., 2016; van Rheenen et al., 2016). Despite this genetic diversity, cytoplasmic aggregates are the pathological hallmark of the disease (Taylor et al., 2016). In the large majority of sporadic ALS cases and all patients with C9orf72 expansion, TDP43, a predominantly nuclear RNA-binding protein, is a major component of these abnormal inclusions (Dion et al., 2009). TDP43 mutations are associated with

Received March 23, 2020. Revised September 16, 2020. Accepted October 4, 2020.

© The Author(s) (2021). Published by Oxford University Press on behalf of Journal of Molecular Cell Biology, CEMCS, CAS.

This is an Open Access article distributed under the terms of the Creative Commons Attribution Non-Commercial License (<http://creativecommons.org/licenses/by-nc/4.0/>), which permits non-commercial re-use, distribution, and reproduction in any medium, provided the original work is properly cited. For commercial re-use, please contact journals.permissions@oup.com

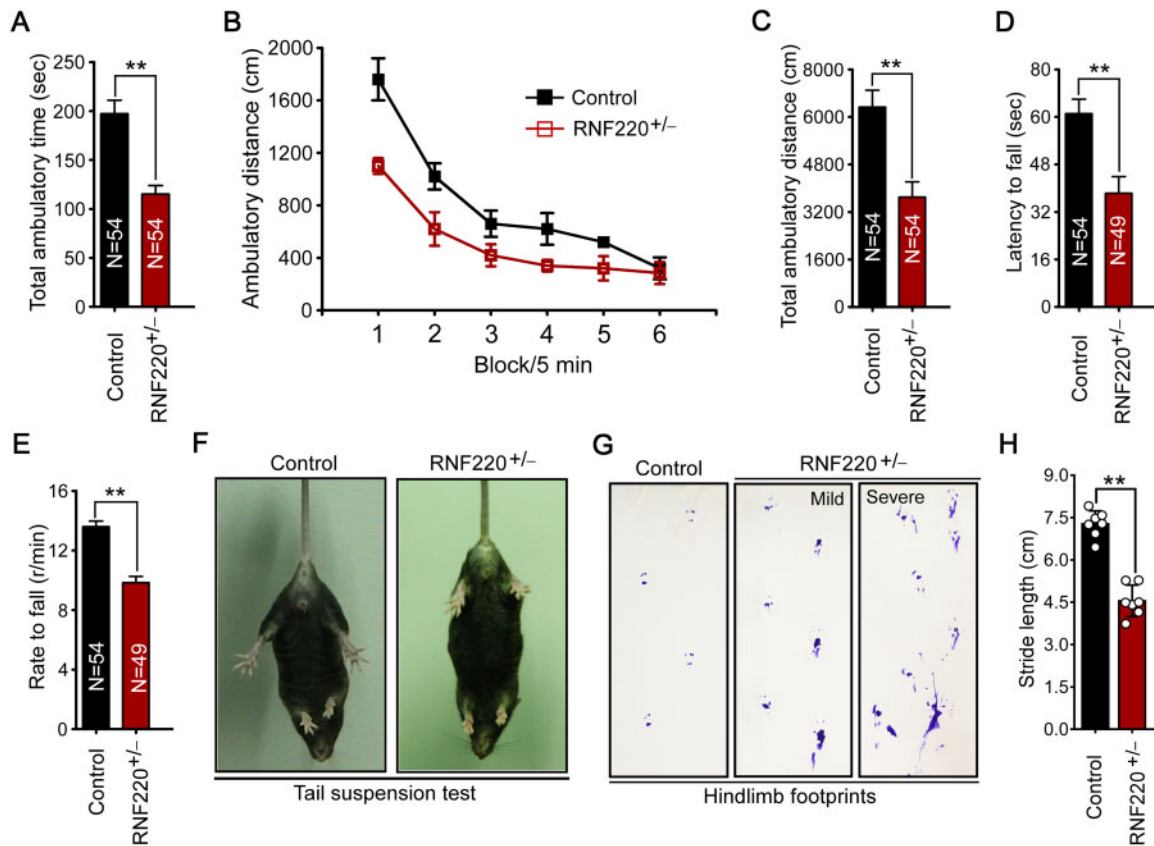


**Figure 1** RNF220<sup>+/-</sup> mice show reduced mobility and gradually develop hindleg paralysis. (A–C) Mouse performances in open field test, including total ambulatory time (A), the moving distance during every 5-min stocks (B), and total ambulatory distance (C). (D and E) Mouse performances in rotarod test, including latent time on a running rotarod (D) and the maximal rate when mice fell on an accelerated rotarod (E). (F) Representative pictures showing hindlimb extension when control and affected RNF220<sup>+/-</sup> mice were suspended by tail tips. (G and H) Hindlimb footprints of wild-type and affected RNF220<sup>+/-</sup> mice. (G) Affected RNF220<sup>+/-</sup> mice exhibit disrupted gait patterns of different degrees (mild and severe). (H) Stride lengths of wild-type and affected RNF220<sup>+/-</sup> mice were measured and shown. \*\**P* < 0.01.

1%–4% of familial and sporadic ALS and rare cases of frontotemporal dementia (FTD) (Dion et al., 2009). Neurons that contain cytoplasmic TDP43 inclusions often have markedly reduced TDP43 staining in the nucleus (Geser et al., 2010; Mackenzie et al., 2010; Lee et al., 2012). TDP43 cleavage by caspases and calpain proteins have been reported to contribute to the formation of TDP43 cytoplasmic toxic aggregates (Yamashita et al., 2012; Li et al., 2015; Yin et al., 2019). The ubiquitin E3 ligase Parkin is also involved in TDP43 metabolism, including its cytoplasmic accumulation, by targeting TDP43 for both K48- and K63-linked polyubiquitination (Hebron et al., 2013). However, Parkin-mediated ubiquitination of TDP43 has no clear effect on its degradation or clearance (Hebron et al., 2013). Znf179 has been identified as an ubiquitin E3 ligase for TDP43 that promotes its turnover, and knockout of Znf179 results in cytoplasmic accumulation of TDP43 in the mouse brain (Lee et al., 2018). Through a proteomics analysis, several ubiquitination sites have been identified within or near the RNA recognition motif 1 (RRM1) domain of TDP43 and suggested to be involved in the regulation of its solubility (Dammer et al., 2012). However, the ubiquitin ligases involved remain unknown.

Therefore, the regulation by ubiquitination may play critical roles in TDP43 proteinopathy and has been suggested to be potential therapeutic target in related diseases.

Here, we report that RNF220<sup>+/-</sup> mice showed reduced mobility and some of the RNF220<sup>+/-</sup> mice progressively developed pathology of ALS-like disease, including hindlimb paralysis, cytoplasmic TDP43 accumulation in motor neurons, muscle wasting, and denervation. Furthermore, we provided evidence that RNF220 specially interacts with and targets TDP43 for K48-linked polyubiquitination and thus controls TDP43 stability both *in vitro* and *in vivo*.

## Results

### RNF220 heterozygotes develop ALS-like phenotype

We and Kim et al. (2018) previously reported that RNF220<sup>-/-</sup> mice are neonatal lethal with neural development defects (Ma et al., 2019, 2020b; Song et al., 2020), while the spinal patterning and cerebellum development are normal in the RNF220<sup>+/-</sup> mouse embryos (Ma et al., 2019, 2020b). Furthermore, we observed progressively reduced motility of

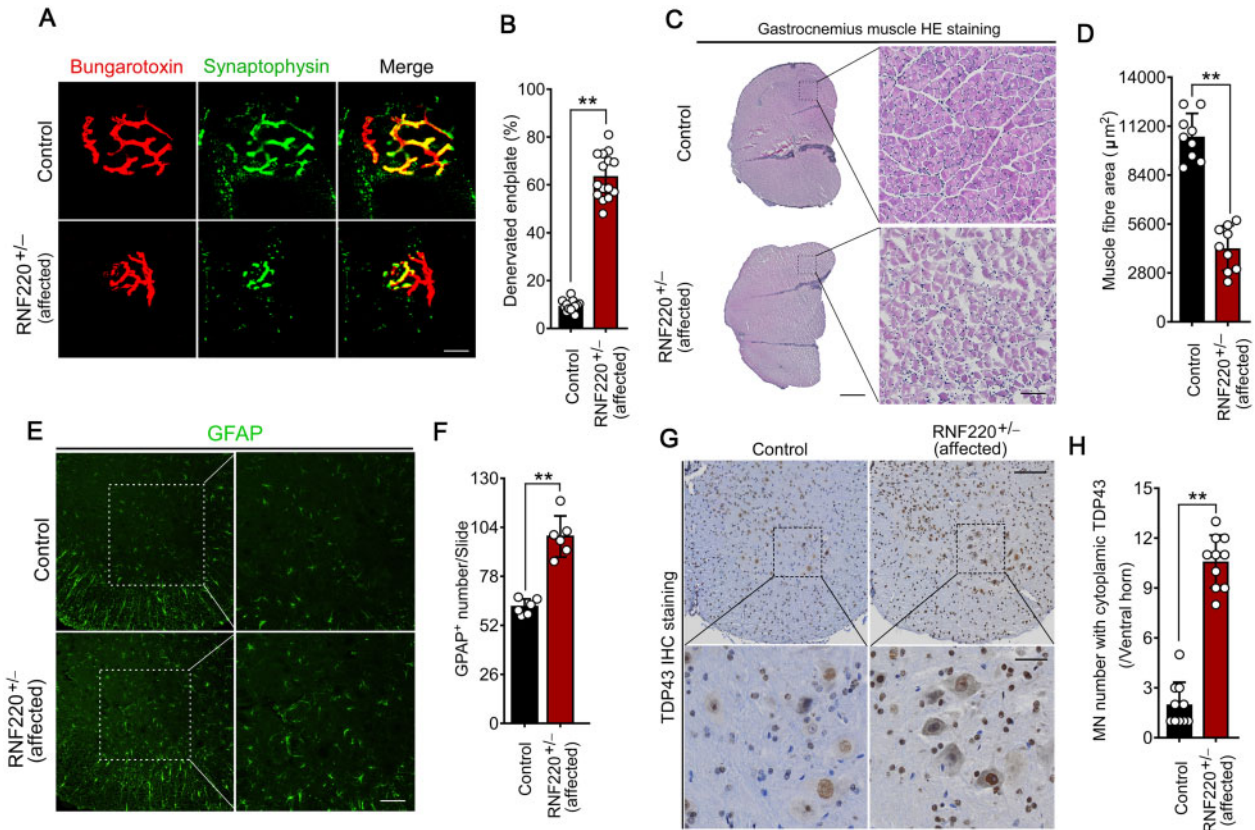


**Figure 2** RNF220<sup>+/-</sup> mice develop ALS-like pathological characteristics. **(A and B)** Representative images of innervation of the tibialis anterior and soleus muscles in control and affected RNF220<sup>+/-</sup> mice. Synaptophysin immunostaining marks presynaptic vesicles in green and bungarotoxin staining marks postsynaptic Ach receptors in red. Scale bar, 5  $\mu$ m. The statistics are shown in **B**. **(C and D)** HE staining on cross-sections of gastrocnemius muscle. Clustered strophic fibers were contained in affected RNF220<sup>+/-</sup> muscle, whereas control mice displayed relatively uniform fiber size. Scale bar, 800  $\mu$ m for left panels and 90  $\mu$ m for right panels. The quantification on fiber area was analyzed and the statistics are shown in **D**. **(E and F)** IF staining showing the number of GFAP-positive astroglia in spinal ventral horns of control and affected RNF220<sup>+/-</sup> mice. Scale bar, 20  $\mu$ m. The statistics are shown in **F**. **(G and H)** IHC staining showing the protein level and distribution of TDP43 in spinal motor neurons of control and RNF220<sup>+/-</sup> mice. The below panels are the amplified views of the boxed areas in the upper panels. Scale bar, 110  $\mu$ m for the upper panels and 50  $\mu$ m for the below panels. The statistics are shown in **H**. At least three pairs of mice (control and affected RNF220<sup>+/-</sup> mice) were examined for these assays and the same results were obtained. \*\* $P < 0.01$ .

RNF220<sup>+/-</sup> mice during postnatal development. Approximately, one-third (34/108) of RNF220<sup>+/-</sup> mice showed severely delayed development and gradually died before 2 months of age (Supplementary Figure S1). For all the survived RNF220<sup>+/-</sup> mice, we tracked their movement performance in open field and on rotarod apparatus at 2–3 months of age. Statistically significant reductions in the outcomes were observed in both tests compared with control animals (Figure 1A–E). From 2 to 6 months of age, one-third (27/87, referred to as ‘affected’ ones hereafter) of them showed increasing hindlimb clasp and gradually developed hindleg paralysis (Figure 1F–H; Supplementary Movies S1 and S2). During the end stage, these affected mice either died spontaneously or were euthanized if they were unable to obtain food or water (Supplementary Movie S3).

We next examined whether the affected RNF220<sup>+/-</sup> mice developed defects in motor neuron, muscle innervation, and

wasting. We quantified the number of motor neurons in the ventral horn of the spinal cord at the end-age stage in the affected RNF220<sup>+/-</sup> and control mice. Motor neurons were identified in the ventral horn by their multipolar shape, large size, and the presence of a prominent nucleolus following hematoxylin–eosin (HE) staining (Supplementary Figure S2A). They were also confirmed by positive choline acetyl transferase (ChAT) staining (Supplementary Figure S2D). No significant change was observed in the number of spinal motor neurons between the affected RNF220<sup>+/-</sup> and control mice (Supplementary Figure S2). We then measured the innervation of neuromuscular junctions of the gastrocnemius muscle by analyzing the extent of colocalization of synaptophysin and  $\alpha$ -bungarotoxin. The results showed that more denervated end plates were observed in the affected RNF220<sup>+/-</sup> mice compared with the controls (Figure 2A and B). Muscle histology from the affected RNF220<sup>+/-</sup> mice showed scattered and group atrophic muscle

fibers, as characterized in muscles from patients with ALS (Hill et al., 2016; Le et al., 2016). HE staining results showed severe muscle wasting in the affected RNF220<sup>+/-</sup> mice compared with the controls (Figure 2C). And the affected RNF220<sup>+/-</sup> mice at the end stage had significantly smaller muscle fiber diameter compared with controls (Figure 2C and D). Furthermore, many of the muscle fibers in RNF220<sup>+/-</sup> mice were triangular rather than in a round shape (Figure 2C), suggestive of degeneration.

We also examined the spinal cord of control and affected RNF220<sup>+/-</sup> mice to see whether there was a change in microglia and astrocyte activation at the end stage. By immunofluorescence (IF) staining, we found a significant increase in GFAP immunoreactivity, indicative of astrocytosis in the affected RNF220<sup>+/-</sup> mice compared with the controls (Figure 2E and F). Microglia activation analysis using Iba1 reactivity revealed increased Iba1 immunoreactivity in the affected RNF220<sup>+/-</sup> spinal cord, compared with the same aged controls (Supplementary Figure S3).

Cytoplasmic aggregates of TDP43, together with loss of normal nuclear TDP43 staining, are common features in vulnerable neurons in ALS (Barmada and Finkbeiner, 2010; Lee et al., 2012). Immunohistochemical (IHC) analysis of TDP43 revealed accumulated cytoplasmic TDP43 staining in the spinal motor neurons in the affected RNF220<sup>+/-</sup> mice compared with the controls (Figure 2G and H). Loss of nuclear TDP43 staining was occasionally seen in the affected RNF220<sup>+/-</sup> spinal motor neurons, similar to what has been reported in ALS patients.

Collectively, we conclude that part of the aged RNF220<sup>+/-</sup> mice spontaneously developed ALS-like cellular and molecular pathological phenotypes.

#### RNF220 regulates TDP43 stability in spinal motor neurons

We tested whether RNF220 interacts with TDP43. When co-transfected in HEK293 cells, TDP43 was pulled-down with RNF220 efficiently, which was also true in the reverse experiment (Figure 3A and B). When TDP43 was immunoprecipitated from wild-type mouse spinal cord lysate using an anti-TDP43 antibody, endogenous RNF220 was also detected in the immunoprecipitate (Figure 3C). To map the domains of RNF220 and TDP43 that are responsible for the observed interaction, a series of RNF220 and TDP43 truncates were tested via immunoprecipitation (IP) assays in HEK293 cells. The results showed that the N-terminal and RING domains of RNF220 and the RRM domains (either RRM1 or RRM2) of TDP43 are likely involved in their interaction (Figure 3D–G).

Furthermore, co-expression of wild-type RNF220, but not its  $\Delta$ RING or the ligase-dead W539R mutant, reduced TDP43 protein level (Figure 4A). The TDP43 aggregates have been reported to be cleared by both the proteasome system and the autophagy pathway (Urushitani et al., 2010; Tashiro et al., 2012; Barmada et al., 2014; Scotter et al., 2014). We tested the pathways potentially involved in RNF220-mediated TDP43 degradation. MG132, a proteasome inhibitor, strongly inhibited

the effect of RNF220 to destabilize TDP43, while the lysosome inhibitor NH<sub>4</sub>Cl and the autophagy inhibitor Chloroquine (CQ) have weaker effects (Figure 4B). We confirmed that the level of polyubiquitinated TDP43 increased when co-expressed with wild-type RNF220, but not the  $\Delta$ RING or ligase-dead mutant (Figure 4C). Ubiquitin ligases can add different types of ubiquitin chains to their substrates with different functional effects (Swatek and Komander, 2016). K48-linked polyubiquitination chains target proteins for proteasomal degradation (Swatek and Komander, 2016). We used different ubiquitin mutants to characterize the type of ubiquitin chains added by RNF220 to TDP43. When the K48R ubiquitin was used, in which the lysine 48 is substituted by an arginine, RNF220 no longer promoted TDP43 for polyubiquitination. On the contrary, when the K48 mutant was used, in which all the lysines but lysine 48 are substituted by arginines, RNF220 efficiently promoted TDP43 for polyubiquitination (Figure 4D). The results showed that RNF220 promotes K48-linked polyubiquitination of TDP43, consistent with the proteasome-dependent proteolytic nature of the modification (Swatek and Komander, 2016). We further tested the effects of RNF220 overexpression on the polyubiquitination of various TDP43 truncates to identify the minimal domains required for its ubiquitination. The RRM1 domain was found to be sufficient for RNF220-mediated polyubiquitination (Supplementary Figure 4A). A series of lysines (lysines 114, 121, 136, 137, 140, 145, and 160) in this region were further mutated to verify the lysine residues ubiquitinated by RNF220. The results showed that lysine 121 is responsible for the polyubiquitination by RNF220, as when it was mutated to arginine, TDP43 could no longer be ubiquitinated by RNF220 (Supplementary Figure S4B).

We tested whether RNF220 regulates TDP43 stabilization and polyubiquitination *in vivo*. Immunoblotting (IB) analysis showed that TDP43 protein level was strongly elevated, while the polyubiquitinated TDP43 significantly reduced in spinal cords from the end-stage affected RNF220<sup>+/-</sup> mice (Figure 4E and F). Note that, in the unaffected RNF220<sup>+/-</sup> mice that did not go paralysis or RNF220<sup>-/-</sup> embryos, the protein level, polyubiquitination status, and subcellular location of TDP43 in the spinal cords are comparable to that in the control mice (Supplementary Figure S5). Lastly, we confirmed that RNF220 is expressed in the spinal cord motor neurons of adult mice, overlapping with ChAT, a motor neuron marker (Figure 4G). Different from their nuclear localization in the spinal neural progenitors (Ma et al., 2019), RNF220 was found mainly in the cytoplasm in the motor neurons (Figure 4G). We suggest that RNF220 plays a role in TDP43 polyubiquitination *in vivo*, which might act as a modifier during the progress of the ALS-like phenotype in this model.

## Discussion

The behavioral deficits and pathologic changes observed in the affected RNF220<sup>+/-</sup> mice are similar with that reported in

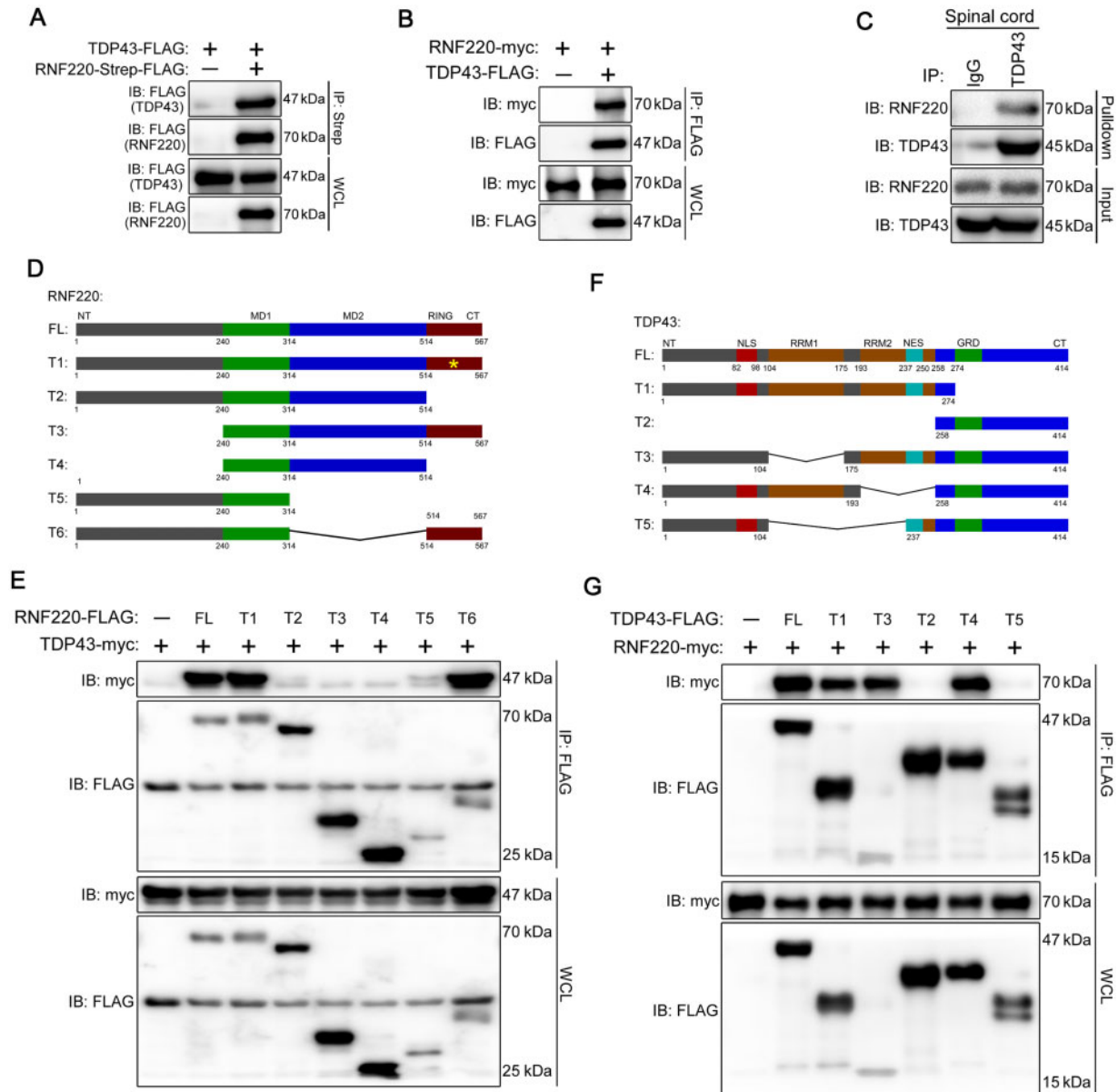


**Figure 3** RNF220 interacts with TDP43 *in vitro* and *in vivo*. **(A and B)** HEK293 cells were transiently transfected with different combinations of expression vectors of TDP43 and RNF220, as indicated. Cell lysates were incubated with streptavidin or anti-FLAG beads, washed, and subsequently analyzed by western blotting. **(A)** TDP43 was immunoprecipitated with RNF220. **(B)** RNF220 was immunoprecipitated with TDP43. **(C)** Endogenous RNF220 could be immunoprecipitated by TDP43 in spinal cord. Lumbar spinal cord tissue extracts were immunoprecipitated with an antibody against TDP43, and endogenous RNF220 was detected by an anti-RNF220 antibody, with IgG as a negative control. **(D)** Schematic representation of the structures of mouse RNF220 truncates. FL, full length; NT, N-terminal; CT, C-terminal; MD1, middle domain 1; MD2, middle domain 2; RING, the catalytic domain RING domain. **(E)** HEK293 cells were transiently transfected with combinations of myc-tagged TDP43 and FLAG-tagged RNF220 or various FLAG-tagged RNF220 truncates. Cell lysates were incubated with anti-FLAG beads and subsequently analyzed by western blotting. Only FL, ligase-dead mutant (T1), and  $\Delta$ MD2 truncate (T6) of RNF220 could associate with TDP43 in co-IP tests. WCL, whole-cell lysate. **(F and G)** Interaction of various TDP43 truncation constructs with RNF220 in co-IP experiments. A schematic map of the TDP43 truncates with amino acid numbers is shown in **F**. NLS, nuclear location signal; NES, nuclear export signal; GRD, glycine-rich domain.

the ALS patients and model animals (Wegorzewska et al., 2009; Le et al., 2016; Archbold et al., 2018; Ebstein et al., 2019). The progressive decrease in rotarod performance in the

RNF220<sup>+/-</sup> lines was associated with progressive loss of muscle innervation of the end plates (Figures 1 and 2). The affected RNF220<sup>+/-</sup> mice showed increased denervated muscle end

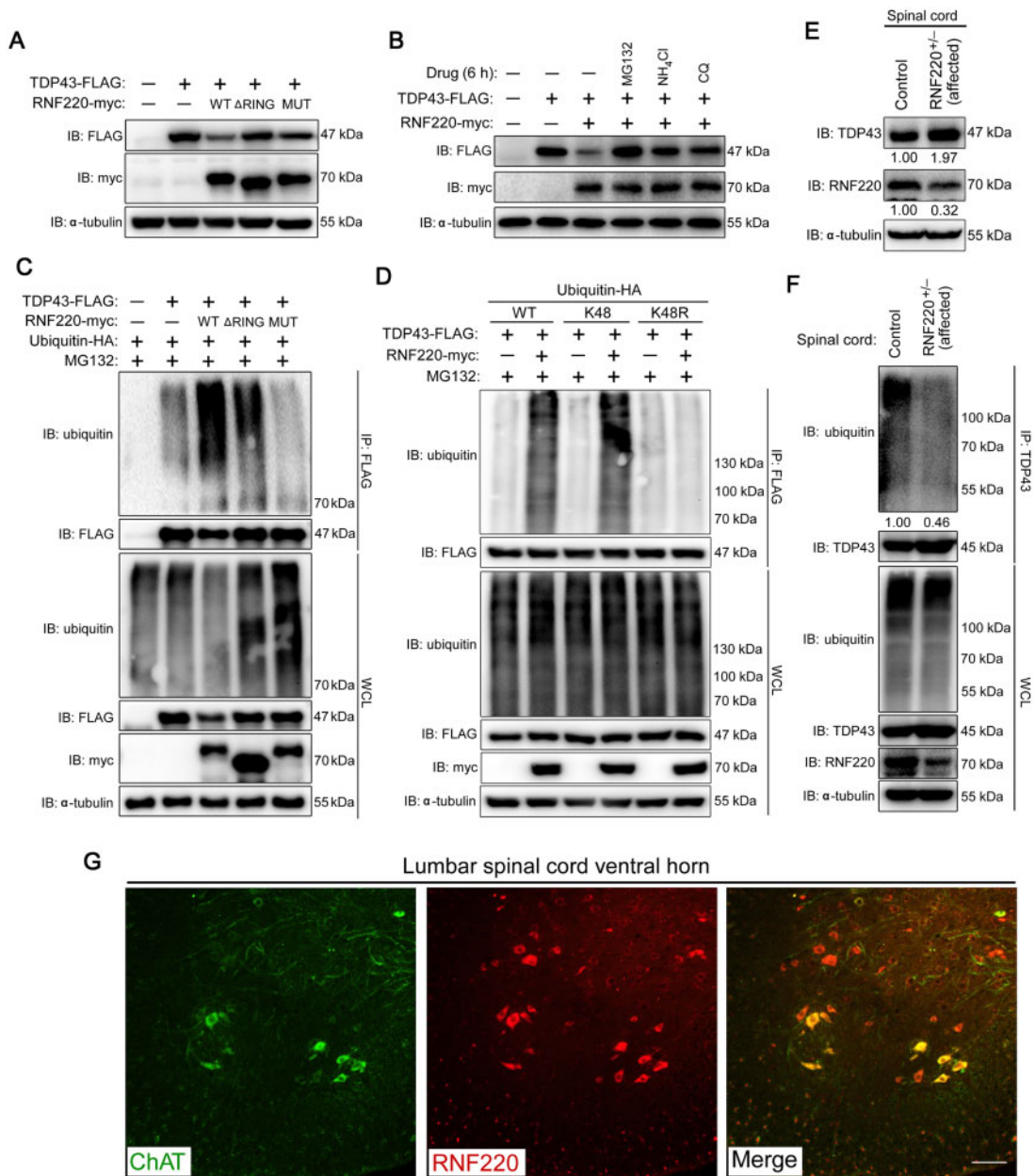


**Figure 4** RNF220 destabilizes TDP43 by targeting it for K48-linked polyubiquitination *in vitro* and *in vivo* and RNF220 expression at spinal motor neurons. **(A)** Wild-type RNF220, but not  $\Delta$ RING or its ligase-dead mutant, destabilized TDP43 protein. FLAG-tagged TDP43 and myc-tagged RNF220 or its truncation plasmids were transfected into HEK293 cells as indicated. After 48 h, cell lysates were analyzed by western blotting. **(B)** The effect of MG132 (a proteasome inhibitor) or  $\text{NH}_4\text{Cl}$  and CQ (inhibitors for the autophagy pathway) treatment on TDP43-destabilizing activity of RNF220. FLAG-tagged TDP43 and myc-tagged RNF220 or its truncation plasmids were transfected into HEK293 cells as indicated. After 40 h, cells were treated with the indicated drugs for another 6–8 h before harvest. Cell lysates were then analyzed by western blotting. **(C)** Ubiquitination assays showing that co-expression of RNF220, but not its  $\Delta$ RING or ligase-dead mutant, enhanced the level of ubiquitinated TDP43 in HEK293 cells. **(D)** Ubiquitination assays showing the ability of RNF220 to ubiquitinate TDP43 when the indicated ubiquitin mutant constructs were used. RNF220 promotes K48-linked polyubiquitination of TDP43. K48R, the K48 of the ubiquitin was mutated to arginine (R); K48, ubiquitin mutants with all lysines except the K48 mutated to arginines. **(E)** Endogenous TDP43 protein was stabilized in the affected RNF220<sup>+/-</sup> spinal cords. The lumbar spinal cord tissue lysates were analyzed by western blotting and the statistics were showed below the indicated blot bands. **(F)** Endogenous levels of polyubiquitinated TDP43 were examined in the affected RNF220<sup>+/-</sup> and control spinal cords. **(G)** IF staining showing the ChAT and RNF220 expression at lumbar spinal cord ventral horns. ChAT labels the motor neurons in the spinal ventral horn and RNF220 is also stained in spinal motor neurons. Scale bar, 50  $\mu\text{m}$ . For assays in **E** and **F**, three pairs of mice (control and affected RNF220<sup>+/-</sup> mice) were examined and the same results were obtained.

plates, muscle wasting, cytoplasmic TDP43 accumulation in spinal motor neurons, and astrocytosis in spinal cord (Figure 2). A remarkable pathological feature found in the affected RNF220<sup>+/-</sup> mice was the presence of TDP43 pathology (i.e. a reduction of TDP43 staining in the nucleus and accumulation in cytoplasmic inclusions) in spinal motor neurons in animals at end stage of the disease. Thus, the affected RNF220<sup>+/-</sup> mice recapitulate well the clinical and pathological phenotypes of human ALS, making it a potential model for understanding the mechanism underlying ALS and for testing therapies to prevent the disease (Swinnen and Robberecht, 2014; Geevasinga et al., 2016; Hardiman et al., 2017).

The RNF220<sup>+/-</sup> mice showed developmental defects to various extents. Approximately, one-third of them die before 2 months of age with severe developmental delay, and one-third of the remaining ones develop ALS-like phenotype as described above. Although having motility defects as revealed in behavior tests, the remaining survived ones develop relatively normal to adult stage. One possible explanation could be that the residual RNF220 level may vary in different individuals and tissues, leading to different penetrances of the phenotype. Intriguingly, the effect of RNF220 knockdown on TDP43 localization/accumulation seems to be specific in spinal motor neurons in the affected animals. Although the 2 to 4-month ‘unaffected’ RNF220<sup>+/-</sup> mice did develop motor defects as detected in behavior tests, no clear TDP43 accumulation was observed in the spinal neurons. It is possible that other parts of the nervous system, such as the motor cortex and brainstem, are also involved in the RNF220-related motor defects, especially in the early postnatal stage. Indeed, we did observe that some of the affected RNF220<sup>+/-</sup> mice develop cerebral edema at end stage. However, the subcellular location of TDP43 in the cortex and hippocampus in these mice are comparable to that in control mice (data not shown), suggesting that additional target(s) must be involved in the observed RNF220<sup>+/-</sup> deficiency. It is reasonable to suggest that RNF220 insufficiency firstly affects motor function without TDP43 proteinopathy, while in those severe cases, TDP43 accumulation was somehow stimulated, leading to further motor neuron toxicity. Other factors are likely involved in such a process. Thus, RNF220 most likely works as a modifier of TDP43 function and ALS progression in this model.

Many TDP43 mutations have been reported to affect the nuclear exclusion and cytoplasmic aggregation of TDP43 (Barmada and Finkbeiner, 2010). Our data here suggest that lysine 121 in the RRM1 domain of TDP43 is the only site for RNF220-mediated polyubiquitination (Supplementary Figure S4). Interestingly, lysine 121 was not identified as an ubiquitination site in a mass spectrometry analysis in HEK293 cells (Dammer et al., 2012). Whether this site is associated with ALS or contributes to ALS progression needs further investigation.

Numerous genetic risk loci have been identified to be associated with ALS based on GWAS and meta-analysis studies (van Rheenen et al., 2016; Chia et al., 2018). RNF220 has not been suggested to be directly associated with ALS, although SNPs in

RNF220 loci were reported to be potential modifiers for ALS (Ahmeti et al., 2012). Our study therefore warrants further study in ALS genetics to test the contribution of RNF220 in ALS and provides a potential mouse model to elucidate ALS biology. Given the wide effects of TDP43 pathology, RNF220-mediated TDP43 ubiquitination may also be involved in other neurodegenerative diseases.

## Materials and methods

### *Mice and genotyping*

All mice were maintained and handled according to guidelines approved by the Animal Care and Use Committee of the Kunming Institute of Zoology, Chinese Academy of Sciences. All mice were maintained on a C57BL/6 background. The conditional RNF220-knockout allele was generated as described previously (Ma et al., 2019). Genotyping by PCR was carried out as reported previously (Ma et al., 2019).

### *Behavioral analysis*

All of the behavioral experiments were approved by the Animal Care and Use Committee of Kunming Institute of Zoology, Chinese Academy of Sciences.

*Tail suspension.* The animal was hung by its tail away from the ground. During this time the animal would try to escape and stretch its limbs. Each animal was tested only once and out of view from the other animals.

*Footprints.* To obtain footprints, the hind feet of the mouse were coated bilaterally with a black nontoxic paint. The animal was then allowed to walk along a 50-cm long, 10-cm wide runway with 10-cm high ways. All mice had two training runs and were then given one run every day. A fresh sheet of paper was placed on the floor of the runway for each run. The footprints patterns were analyzed for three classical step parameters. Stride length was measured as the average distance of forward movement between each stride.

*Open field.* Mice were placed individually in an open-field (OF) arena housed within a sound attenuating cubicle and permitted to move freely. Trials lasted for 30 min. Animal motion and cumulative path length were automatically tracked via three 16-beam infrared array and recorded by the Activity Monitor software.

*Rotarod test.* Mice were tested for time or accelerating speed on rotarod. Three trials were administered in each test. Mice were allowed to have at least 10 min rest between the trials. The best performance among the three trials was recorded as the performance of different genotypes.

### *Cells, plasmids, transfections, IP, ubiquitination assays, and western blotting*

HEK293 cell culture, plasmid transfection, IP, western blotting, and ubiquitination assays were all carried out as

previously described (Ma et al., 2014, 2019). The following antibodies were used for western blotting: RNF220 (1:1000, Sigma, HPA027578); TDP43 (1:1000, ProteinTech, 10782-2-AP); ubiquitin (1:2000, SantaCruz, sc8017); FLAG (1:5000, Sigma, F7425); myc (1:5000, Sigma, C3956); and  $\alpha$ -tubulin (1:5000, ProteinTech, 6603-1-Ig).

All of the TDP43 expression constructs were gifts from Dr Baowei Jiao (Kunming Institute of Zoology, Chinese Academy of Sciences). RNF220 expression constructs were described previously (Ma et al., 2014, 2019). For drug treatments, HEK293 cells were subjected to 15  $\mu$ M MG132 (Sigma), 20 mM NH<sub>4</sub>Cl (Sigma), or 50  $\mu$ M CQ (Chloroquine, Sigma) for 6–8 h before harvested.

#### Sections, HE staining, IF, and IHC

Mice under deep anesthesia were transcardially perfused with cold PBS followed by 4% (w/v) paraformaldehyde in phosphate-buffered saline (PBS). Then, the indicated tissues, including spinal cord and muscles, were dissected out and immersed in the same fixative at 4°C for another 24–28 h. After fixation, tissues were immersed in PBS containing 30% (w/v) sucrose at 4°C for 2–3 days. Tissues were then frozen in optimal cutting temperature (OCT) freezing media (Leica) and stored at –20°C. Frozen sections were cut at 10  $\mu$ m using a cryostat. HE staining was carried out using a kit from Beyotime (C0105) according to the instructions. For muscle HE staining, the fresh tissues were cut immediately using a cryostat without a sedimentation procedure in sucrose solution. IF and IHC assays were carried out as previously described (Ma et al., 2019, 2020b). For neuro-muscle junction staining, 100- $\mu$ m-thick muscle frozen sections were used. The following antibodies or probes were used: anti-RNF220 (1:200, Sigma, HPA027578), anti-GFAP (1:500, Dako, 20334), anti-IBA1 (1:1000, GeneTex, GTX100042), anti-TDP43 (1:200, ProteinTech, 10782-2-AP), anti-Synaptophysin (1:50, ProteinTech, 17785-1-AP), anti-CHAT (1:50, Abcam, ab1449), and a 594-coupled  $\alpha$ -Bungarotoxin probe (1:50; a gift from Dr Yun Zhang, Kunming Institute of Zoology, Chinese Academy of Sciences).

#### Statistical analysis

Statistical analysis was performed using a two-tailed unpaired *t*-test, with *P*-values <0.05 considered statistically significant and *P*-values <0.01 considered statistically very significant. GraphPad software was used for all statistical calculations. All experiments were carried out at least three times and samples were analyzed in at least triplicate.

#### Supplementary material

Supplementary material is available at *Journal of Molecular Cell Biology* online.

#### Acknowledgements

We thank Dr Baowei Jiao (Kunming Institute of Zoology, Chinese Academy of Sciences) for providing TDP43 plasmids,

Dr Yun Zhang (Kunming Institute of Zoology, Chinese Academy of Sciences) for  $\alpha$ -Bungarotoxin probes, and Dr Lin Xu (Kunming Institute of Zoology, Chinese Academy of Sciences) for help with mouse behavior tests. We thank Drs Cheol-Hee Kim (Chungnam National University, Korea) and Hyung-Goo Kim (Hamad Bin Khalifa University, Qatar) for helpful discussions.

#### Funding

This work was supported by the National Natural Science Foundation of China (31671521 and 31871483 to B.M.) and Yunnan Basic Research Program (202001AS070036 to B.M.).

**Conflict of interest:** none declared.

**Author contributions:** B.M. and P.M. designed the experiments. P.M. and Y.L. performed most of the experiments and analyzed the data. H.W. helped with the experiments. P.M. and B.M. wrote the paper.

#### References

- Ahmeti, K.B., Ajroud-Driss, S., Al-Chalabi, A., et al. (2012). Age of onset of amyotrophic lateral sclerosis is modulated by a locus on 1p34.1. *Neurobiol. Aging* 34, 357.e7–357.e19.
- Archbold, H.C., Jackson, K.L., Arora, A., et al. (2018). TDP43 nuclear export and neurodegeneration in models of amyotrophic lateral sclerosis and frontotemporal dementia. *Sci. Rep.* 8, 4606.
- Barmada, S.J., and Finkbeiner, S. (2010). Pathogenic TARDBP mutations in amyotrophic lateral sclerosis and frontotemporal dementia: disease-associated pathways. *Rev. Neurosci.* 21, 251–272.
- Barmada, S.J., Serio, A., Arjun, A., et al. (2014). Autophagy induction enhances TDP43 turnover and survival in neuronal ALS models. *Nat. Chem. Biol.* 10, 677–685.
- Chia, R., Chio, A., and Traynor, B.J. (2018). Novel genes associated with amyotrophic lateral sclerosis: diagnostic and clinical implications. *Lancet Neurol.* 17, 94–102.
- Dammer, E.B., Fallini, C., Gozal, Y.M., et al. (2012). Coaggregation of RNA-binding proteins in a model of TDP-43 proteinopathy with selective RGG motif methylation and a role for RRM2 Ubiquitination. *PLoS One* 7, e38658.
- Dion, P.A., Daoud, H., and Rouleau, G.A. (2009). Genetics of motor neuron disorders: new insights into pathogenic mechanisms. *Nat. Rev. Genet.* 10, 769–782.
- Ebstein, S.Y., Yagudayeva, I., and Shneider, N.A. (2019). Mutant TDP-43 causes early-stage dose-dependent motor neuron degeneration in a TARDBP Knockin mouse model of ALS. *Cell Rep.* 26, e364–e373.
- Galves, M., Rathi, R., Prag, G., et al. (2019). Ubiquitin signaling and degradation of aggregate-prone proteins. *Trends BiochemSci.* 44, 872–884.
- Geevasinga, N., Menon, P., Ozdinler, P.H., et al. (2016). Pathophysiological and diagnostic implications of cortical dysfunction in ALS. *Nat. Rev. Neurol.* 12, 651–661.
- Geser, F., Lee, V.M., and Trojanowski, J.Q. (2010). Amyotrophic lateral sclerosis and frontotemporal lobar degeneration: a spectrum of TDP-43 proteinopathies. *Neuropathology* 30, 103–112.
- Hardiman, O., Al-Chalabi, A., Chio, A., et al. (2017). Amyotrophic lateral sclerosis. *Nat. Rev. Dis. Primers* 3, 17071.
- Hebron, M.L., Lonskaya, I., Sharpe, K., et al. (2013). Parkinubiquitinates Tar-DNA binding protein-43 (TDP-43) and promotes its cytosolic accumulation via interaction with histone deacetylase 6 (HDAC6). *J. Biol. Chem.* 288, 4103–4115.

- Hill, S.J., Mordes, D.A., Cameron, L.A., et al. (2016). Two familial ALS proteins function in prevention/repair of transcription-associated DNA damage. *Proc. Natl Acad. Sci. USA* *113*, E7701–E7709.
- Kim, J., Choi, T.I., Park, S., et al. (2018). Rnf220 cooperates with Zc4h2 to specify spinal progenitor domains. *Development* *145*, dev165340.
- Kong, Q., Zeng, W., Wu, J., et al. (2010). RNF220, an E3 ubiquitin ligase that targets Sin3B for ubiquitination. *Biochem. Biophys. Res. Commun.* *393*, 708–713.
- Le, N.T., Chang, L., Kovlyagina, I., et al. (2016). Motor neuron disease, TDP-43 pathology, and memory deficits in mice expressing ALS-FTD-linked UBQLN2 mutations. *Proc. Natl Acad. Sci. USA* *113*, E7580–E7589.
- Lee, E.B., Lee, V.M., and Trojanowski, J.Q. (2012). Gains or losses: molecular mechanisms of TDP43-mediated neurodegeneration. *Nat. Rev. Neurosci.* *13*, 38–50.
- Lee, Y.C., Huang, W.C., Lin, J.H., et al. (2018). Znf179 E3 ligase-mediated TDP-43 polyubiquitination is involved in TDP-43-ubiquitinated inclusions (UBI) (+)-related neurodegenerative pathology. *J. Biomed. Sci.* *25*, 76.
- Li, Q., Yokoshi, M., Okada, H., et al. (2015). The cleavage pattern of TDP-43 determines its rate of clearance and cytotoxicity. *Nat. Commun.* *6*, 6183.
- Ma, P., An, T., Zhu, L., et al. (2020a). RNF220 is required for cerebellum development and regulates medulloblastoma progression through epigenetic modulation of Shh signaling. *Development* *147*, dev188078.
- Ma, P., Song, N.N., Cheng, X., et al. (2020b). ZC4H2 stabilizes RNF220 to pattern ventral spinal cord through modulating Shh/Gli signaling. *J. Mol. Cell Biol.* *12*, 337–344.
- Ma, P., Song, N.N., Li, Y., et al. (2019). Fine-tuning of Shh/Gli signaling gradient by non-proteolytic ubiquitination during neural patterning. *Cell Rep.* *28*, 541–553.e4.
- Ma, P., Yang, X., Kong, Q., et al. (2014). The ubiquitin ligase RNF220 enhances canonical Wnt signaling through USP7-mediated deubiquitination of  $\beta$ -catenin. *Mol. Cell. Biol.* *34*, 4355–4366.
- Mackenzie, I.R., Rademakers, R., and Neumann, M. (2010). TDP-43 and FUS in amyotrophic lateral sclerosis and frontotemporal dementia. *Lancet Neurol.* *9*, 995–1007.
- Scotter, E.L., Vance, C., Nishimura, A.L., et al. (2014). Differential roles of the ubiquitin proteasome system and autophagy in the clearance of soluble and aggregated TDP-43 species. *J. Cell Sci.* *127*, 1263–1278.
- Song, N.N., Ma, P., Zhang, Q., et al. (2020). Rnf220/Zc4h2-mediated monoubiquitination of Phox2 is required for noradrenergic neuron development. *Development* *147*, dev185199.
- Swatek, K.N., and Komander, D. (2016). Ubiquitin modifications. *Cell Res.* *26*, 399–422.
- Swinnen, B., and Robberecht, W. (2014). The phenotypic variability of amyotrophic lateral sclerosis. *Nat. Rev. Neurol.* *10*, 661–670.
- Tashiro, Y., Urushitani, M., Inoue, H., et al. (2012). Motor neuron-specific disruption of proteasomes, but not autophagy, replicates amyotrophic lateral sclerosis. *J. Biol. Chem.* *287*, 42984–42994.
- Taylor, J.P., Brown, R.H., and Cleveland, D.W. (2016). Decoding ALS: from genes to mechanism. *Nature* *539*, 197–206.
- Urushitani, M., Sato, T., Bamba, H., et al. (2010). Synergistic effect between proteasome and autophagosome in the clearance of polyubiquitinated TDP-43. *J. Neurosci. Res.* *88*, 784–797.
- van Rheenen, W., Shatunov, A., Dekker, A.M., et al. (2016). Genome-wide association analyses identify new risk variants and the genetic architecture of amyotrophic lateral sclerosis. *Nat. Genet.* *48*, 1043–1048.
- Wegorzewska, I., Bell, S., Cairns, N.J., et al. (2009). TDP-43 mutant transgenic mice develop features of ALS and frontotemporal lobar degeneration. *Proc. Natl Acad. Sci. USA* *106*, 18809–18814.
- Yamashita, T., Hideyama, T., Hachiga, K., et al. (2012). A role for calpain-dependent cleavage of TDP-43 in amyotrophic lateral sclerosis pathology. *Nat. Commun.* *3*, 1307.
- Yin, P., Guo, X., Yang, W., et al. (2019). Caspase-4 mediates cytoplasmic accumulation of TDP-43 in the primate brains. *Acta Neuropathol.* *137*, 919–937.
- Zhang, L., Ye, M., Zhu, L., et al. (2020). Loss of ZC4H2 and RNF220 inhibits neural stem cell proliferation and promotes neuronal differentiation. *Cells* *9*, 1600.